Supporting Information

Choi et al. 10.1073/pnas.1105116108

SI Text

Ultrasound Transducer Calibration. Peak-rarefactional pressure amplitudes were measured with a hybrid needle-membrane hydrophone (diameter: 0.2 mm; Onda) in degassed water while accounting for 18% attenuation through the parietal bone of the mouse skull (1, 2). The 3.5-cycle pulse shape is depicted in Fig. S1 and the lateral and the axial FWHM peak-rarefactional pressure were 1.3 and 10.5 mm, respectively.

Brain Preparation and Fluorescence Microscopy. Approximately 20 min after injection of the combined microbubble and dextran formulation, which corresponded to 10 min after the end of sonication, the mice were transcardially perfused with 30 mL of phosphate buffer saline (138 mM sodium chloride, 10 mM phosphate, pH 7.4) and then 60 mL of 4% paraformaldehyde (PFA). The brain, which remained encased in the skull, was soaked in 4% PFA and then extracted from the skull the next day and separately soaked in 4% PFA for an additional day.

Eighty-seven of the brains were serially diluted in 10%, 20%, and then 30% sucrose at 30 min, 1 h, and overnight time increments, respectively. They were then embedded in a formulation of water-soluble glycols and resins (Sakura Tissue-Tek O.C.T. Compound), frozen in a square mold, and sectioned using a cryostat into 100-μm slices in the horizontal orientation. Images of all frozen sections were then acquired using an upright fluorescence microscope (excitation: 568 ± 24 nm; emission: 610 ± 40 nm; BX61; Olympus) and select sections were also imaged using a confocal fluorescence microscope (Leica).

Four dorsal sections, four ventral sections, and a reference midline section, which was determined by anatomical landmarks, were selected for analysis. Sections with preparation or sectioning artifacts (e.g., separation of the hippocampus from the thalamus, overlapping brain tissue due to folding, etc.) were excluded from analysis and replaced by a neighboring section. The focused ultrasound (FUS)-targeted (left) and control (right) region of interest (ROI) of a section, were manually outlined using Matlab (Fig. S2 *C–E*) and utilized to quantify the extent of dextran delivery.

The fluorescence images were processed in order to quantify (*i*) a normalized optical density (NOD) value that represented a relative increase in the amount of dextran delivered to the target ROI and (*ii*) the probability of dextran delivery occurring given an experimental condition. Every fluorescence image was normalized by dividing each image by the spatial average of the right (nonsonicated) hippocampus as determined using the manual outlines (Fig. S2). Fluorescence pixel intensities due to dextran delivery were separated from background brain autofluorescence by applying a threshold defined as an intensity of twice the standard deviation of the right (control) hippocampus. Fluorescent pixels were then summed in their respective hemispheric ROIs for all sections of a given brain. The left hemispheric summation value was then subtracted by its contralateral right hemispheric value to provide the NOD value. For each brain, the NOD thus approximated the sum of all pixels with fluorescence above the set threshold that indicated delivery of dextran. A NOD value for each of the 27 ultrasonic parameters was then obtained by averaging the NOD of all mice exposed under specific parameters (Table S1).

Successful in vivo dextran delivery was determined in each mouse brain if its NOD was higher by at least one standard deviation relative to the NODs of the sham experimental condition. The probability of dextran delivery was then calculated as the number of mouse brains exposed to a given experimental condition yielding successful delivery divided by the total number of mouse brains exposed.

The mean and standard deviation of NOD across the three mice were calculated for each experimental condition. A difference in NOD between two sets of experimental conditions was determined to be significant if the P value was less than 0.05 using a two-sided Student's t test. A significant increase in NOD was determined when comparing to the no FUS control. The incidence of NOD increase within a given experimental condition was determined by comparing the target left ROI to the right ROI.

Magnetic Resonance Imaging. Mice were imaged in a 30-mm diameter birdcage coil and 9.4-T MRI system (DRX400, Bruker Biospin) approximately 60 min after FUS treatment. Dynamic contrast-enhanced (DCE) MR images were acquired with a T1-weighted 2D fast low angle shot (FLASH) sequence (time to repetition (TR)/time to echo (TE) = 230/3.3 ms, flip angle: 70°, number of excitations (NEX): 4, scan time: 88 s, matrix size: 192×128, reconstructed size: 256×128, resolution: 130×130 μm^2, reconstructed resolution: 98×130 μm^2, slice thickness: 600 μm, no interslice gap). Forty sequential images were acquired over a time window of 60 min. Gadodiamide (0.3 mL; Omniscan®, GE Healthcare) was administered via an intraperitoneal catheter at the end of the second image acquisition. Higher spatial resolution images were then acquired with T1-weighted 2D FLASH (TR/TE = 230/2.9 ms, flip angle: 70°, NEX: 18, scan time: 9 min 56 s, matrix size: 256×192, spatial resolution: 86×86 μm^2, slice thickness: 500 μm, no interslice gap) and T2-weighted 2D rapid acquisition with relaxation enhancement (RARE) (TR/TE = 3,300/43.8 ms; echo train: 8; NEX = 10; scan time: 9 min 54 s; matrix size: 256×192; spatial resolution: 86×86 μm^2; slice thickness: 500 μm, no interslice gap) sequences.

Vascular permeability maps of the blood–brain barrier (BBB) disruption was quantified with the DCE-MR images using previously developed methods (3). In brief, the generalized form of the Tofts and Kermode bidirectional model or general kinetic model (GKM) was used and is described by the following general expression: $\frac{dC_t}{dt} = K_{\text{trans}} C_p - K_{ep} C_t$, where C_t is the tracer concentration in the extracellular extravascular space (EES), t is the time, C_p is the tracer concentration in the blood plasma, and K_{trans} and K_{ep} are the transfer and efflux rate constants from the intravascular system to the EES and from the EES to the intravascular system, respectively. The tracer concentration in the blood plasma was estimated by fitting a population-averaged arterial input function (AIF) for 33 mice to a biexponential model (3). The tracer concentration in the EES for each MRI voxel was estimated using the DCE-MR images. The two tracer concentration values were then used to estimate K_{trans} and K_{ep} for every voxel or selected ROI. All the images were smoothed before the concentration fitting, using a 3×3 linear filter. Major vessels were excluded in the fitting wherever possible, by avoiding the corresponding regions, where the concentration followed an exponential decaying pattern, similar to the one recorded for the AIF. Moreover, whenever GKM converged to negative or very high (>30 min) estimated gadolinium diethylenetriamine pentaacetic acid (Gd-DTPA) injection times, the permeability values were discarded, because the i.p. injection always started at approximately $t = 3$ min after the DCE-MRI acquisition.

Histological Analysis. Eight brains were prepared by using standard sectioning and paraffin embedding procedures. A total of seventy-two 6-μm-thick sections at 12 different levels were obtained. At each level, 2 sections were H&E-stained, 2 sections were TUNEL-stained, and 2 sections remained unstained. The TUNEL assay was performed using the DeadEnd Colorimetric TUNEL system (Promega), and sections were counterstained in Harris hematoxylin. Bright field microscopy of the H&E- and TUNEL-stained sections was used to assess damage, whereas fluorescence microscopy of the unstained sections was used to confirm successful dextran delivery to the target ROI.

1. Choi JJ, Pernot M, Small SA, Konofagou EE (2007) Noninvasive, transcranial and localized opening of the blood-brain barrier using focused ultrasound in mice. *Ultrasound Med Biol* 33:95–104.
2. Choi JJ, Pernot M, Brown TR, Small SA, Konofagou EE (2007) Spatio-temporal analysis of molecular delivery through the blood-brain barrier using focused ultrasound. *Phys Med Biol* 52:5509–5530.
3. Vlachos F, Tung YS, Konofagou E (2011) Permeability dependence study of the focused ultrasound-induced blood-brain barrier opening at distinct pressures and microbubble diameters using DCE-MRI. *Magn Reson Med* 66:821–830.

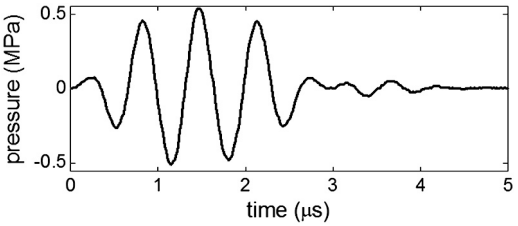

Fig. S1. The shape of the 3.5-cycle ultrasonic pulse emitted from the focused ultrasound transducer.

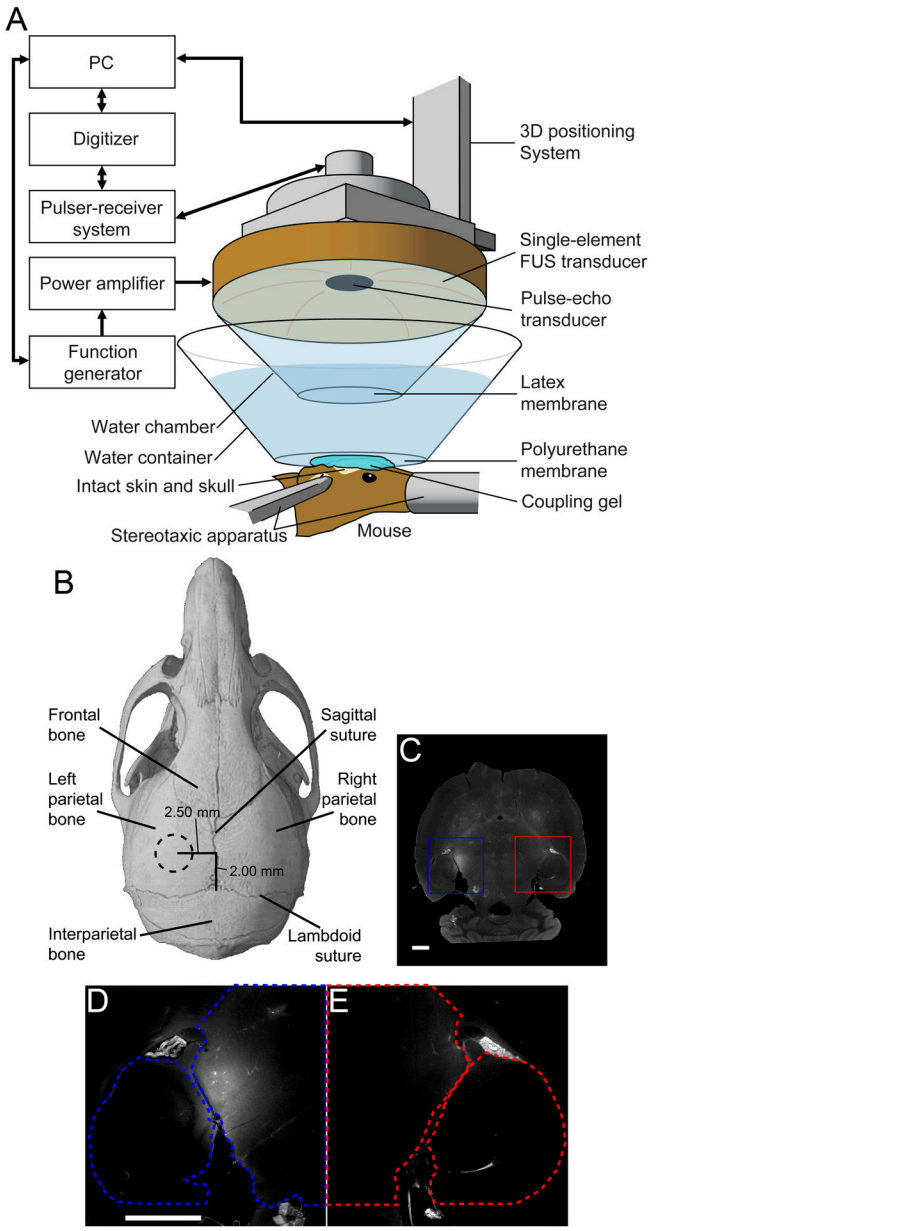

Fig. S2. Experimental setup and focused ultrasound-targeted regions of interest. (*A*) The mouse brain was sonicated in vivo through the intact skin and skull using a single-element focused ultrasound transducer. In the presence of systemically administered microbubbles and fluorescently tagged 3-kDa dextran, ultrasonic pulses of 3.5 cycles were targeted through the (*B*) parietal bone of the mouse skull and converged to a (*C*) region in the left hemisphere (blue square) containing the left hippocampus and lateral thalamus. (*D*) An increase in fluorescence within the targeted region was observed relative to the right control region. *D* and *E* are magnifications of the blue and red squares in *C*. The dotted blue and red regions in *D* and *E* correspond to ROIs outlined to calculate the normalized optical density. The scale bars in *C* and *D* depict 1 mm in length.

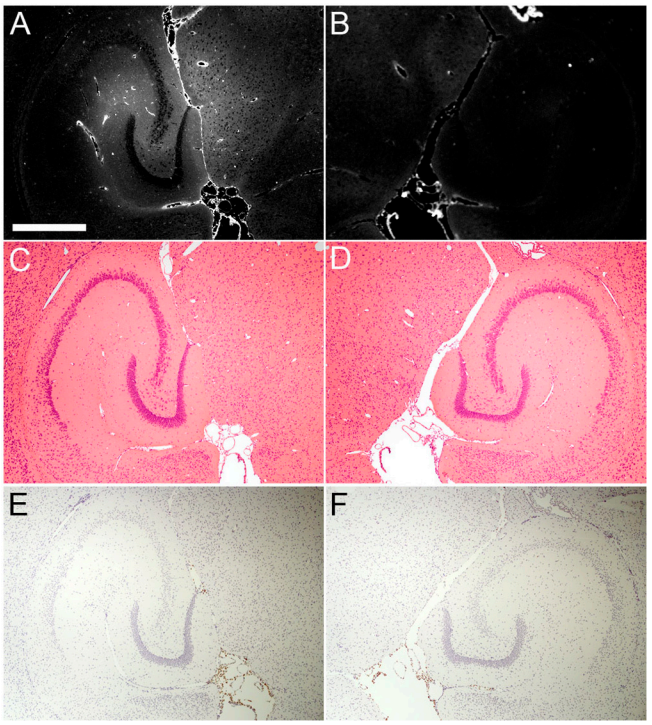

Fig. S3. Paraffin-embedded fluorescence unstained bright field H&E-stained, and TUNEL-stained sections. The left ROI of the mouse brain was exposed to 3.5-cycle pulses of FUS in the presence of systemically administered microbubbles and fluorescently tagged 3-kDa dextran. Fluorescence images of the (*A*) targeted left ROI depict increases in fluorescence, whereas the (*B*) right control ROI does not. The immediate neighboring sections of the unstained fluorescence images were stained with (*C* and *D*) H&E and (*E* and *F*) TUNEL. No differences in either the number of erythrocyte extravasations or dark neurons were observed in the (*C*) left H&E-stained sections compared to the (*D*) right control. (*E* and *F*) No difference in TUNEL-positive cells was observed either. In particular, the regions of high fluorescence in *A* have no indication of damage in *C* and *E*. The white bar in *A* depicts 1 mm.

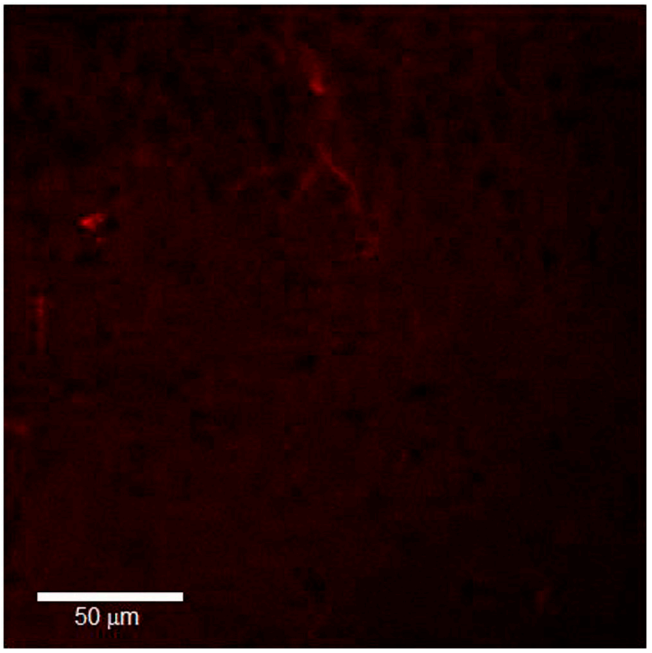

Movie S1. Multiple 2D confocal microscopy images shown at variable depths within the targeted region of interest. One of these images is shown in Fig. 5*H* in the main text. I.v.-administered 3-kDa dextran molecules are shown to be not only homogeneously distributed, but also targeted to neurons or glial cells and capillaries.

Movie S1 (MOV)

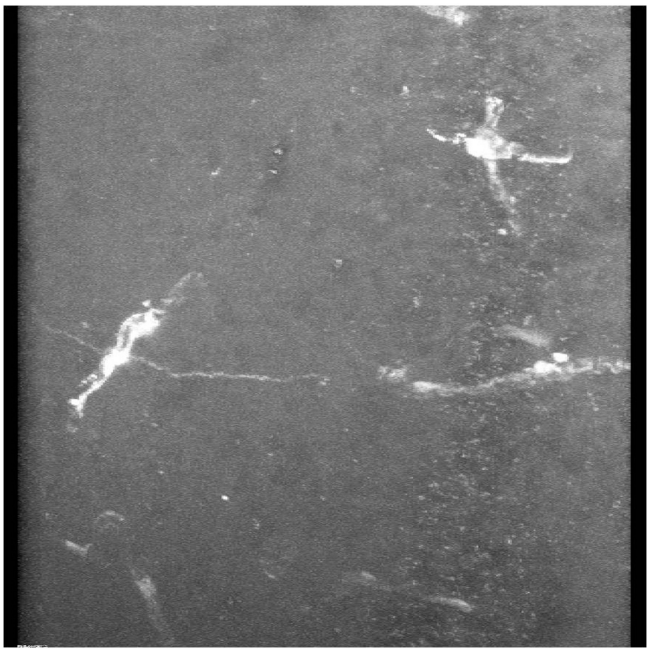

Movie S2. Three-dimensional reconstruction of the 2D images shown in Movie S1 showing the links between the fluorescent neurons over multiple regions in the brain. The fluorescent 3-kDa dextran was capable of penetrating through the BBB and into the neurons or glial cells and capillaries through the blood–brain barrier.

Movie S2 (MOV)

Table S1. Ultrasonic parameters the mouse brain was exposed to in vivo

Pulse repetition frequency, kHz	Burst repetition frequency, Hz	Burst length, # of pulses	Peak-rarefactional pressure	NOD x 1e9 (mean ± SD)	Incidence of NOD increase
—*	—*	—*	0	0.02 ± 0.19	0/3
100	—†	—†	0.51	0.21 ± 0.32	1/3
100	10	1,000	0.51	2.01 ± 1.44	3/3
100	5	1,000	0.51	6.14 ± 1.45	3/3
100	2	1,000	0.51	3.08 ± 2.76	3/3
100	1	1,000	0.51	1.45 ± 0.73	3/3
100	0.1	1,000	0.51	0.99 ± 0.85	2/3
25	—†	—†	0.51	0.30 ± 0.20	1/3
25	10	1,000	0.51	1.31 ± 1.35	2/3
25	5	1,000	0.51	1.48 ± 0.77	3/3
25	2	1,000	0.51	3.34 ± 1.35	3/3
25	1	1,000	0.51	1.92 ± 0.10	3/3
25	0.1	1,000	0.51	0.35 ± 0.10	2/3
6.25	—†	—†	0.51	−0.11 ± 0.35	1/3
6.25	5	1,000	0.51	0.56 ± 0.95	2/3
6.25	2	1,000	0.51	−0.16 ± 0.67	1/3
6.25	1	1,000	0.51	0.78 ± 0.85	2/3
6.25	0.1	1,000	0.51	0.68 ± 0.47	2/3
100	5	1,000	0.37	0.60 ± 0.48	2/3
100	5	1,000	0.25	0.10 ± 0.16	1/3
100	5	1,000	0.13	0.10 ± 0.21	1/3
100	5	500	0.51	3.30 ± 0.58	3/3
100	5	100	0.51	3.60 ± 0.95	3/3
100	5	50	0.51	2.20 ± 0.54	3/3
100	5	10	0.51	2.14 ± 1.33	3/3
100	5	5	0.51	0.13 ± 0.17	1/3
100	5	1	0.51	0.01 ± 0.11	0/3

All parameters used a 3.5-cycle pulse length and a sonication duration of 11 min. For each experimental condition, the NOD was calculated as a measure of increased fluorescence in the left (targeted) ROI compared to the right (control) ROI.
*Sham mice where no ultrasound was applied.
†Parameters where pulses were emitted continuously and without bursts.